

Relaxation Dynamics of a Liquid in the Vicinity of an Attractive Surface: The Process of Escaping from the Surface

Alireza F. Behbahani^{1,2,*} and Vagelis Harmandaris^{3,2,4}

¹*Institut für Physik, Johannes Gutenberg-Universität Mainz, Staudingerweg 7, D-55099 Mainz, Germany*

²*Institute of Applied and Computational Mathematics,*

Foundation for Research and Technology - Hellas, Heraklion GR-71110, Greece

³*Computation-based Science and Technology Research Center, The Cyprus Institute, Nicosia 2121, Cyprus*

⁴*Department of Mathematics and Applied Mathematics,
University of Crete, Heraklion GR-71110, Greece*

We analyze the displacements of the particles of a liquid perpendicular to an attractive confining surface, using extensive molecular dynamics simulations. Because of the attraction of the surface, the particles are trapped in its vicinity. This leads to a three-step relaxation of the liquid close to the surface. The first step is related to the rattling motions of the particles in the cages formed by their nearest neighbors; the second step is related to small-scale movements close to the surface, and the third step is associated with the process of escaping from the surface. The three-step relaxation is seen through the self-intermediate scattering function or the mean squared displacement of the particles. Upon reducing temperature, the second and third relaxation steps seem to be gradually merged. The solid surface induces also a strong heterogeneity in the mobility of its adjacent particles. This can be seen from the large peak of the non-Gaussian parameter for the particle displacements, which concurs with the appearance of the third step in the relaxation functions. The surface-induced dynamical heterogeneity increases with decreasing temperature.

The dynamics of confined glass-forming liquids has been extensively studied computationally [1–9] and experimentally [10–15]. These studies are partly motivated by the technological importance of understanding the behavior of these materials. Furthermore, confined systems have been studied in order to gain insight into the mechanism of glassy dynamics and the nature of glass transition temperature, T_g [16, 17].

Some features of the dynamics of glass-forming liquids are usually discussed based on the so-called cage effect [18–21]. According to it, at short times, a particle of the liquid is trapped in a temporary cage formed by its neighboring particles. At intermediate times, some of the particles escape from their cages while some of them are still restricted in the cages; this leads to the heterogeneity of particle displacements within the liquid which can be recognized from the peak of the non-Gaussian parameter for the particle displacements [22–25]. The cage effect leads to a two-step relaxation of the liquid; a short-time step that comes from fast movements within the cage and a long-time step that appears after cage breaking (α -relaxation) [19]. The two-step relaxation can be seen through the two-step decay of, for example, self intermediate scattering function or through the two-step increase of mean-squared displacement with time [19, 26].

Previously, for interfacial polymer systems, three-step decay of self-intermediate scattering function was observed and discussed as a polymer-specific phenomenon [27, 28]. In this letter, we show that this phenomenon is not limited to polymers. Also, besides the scattering function, we show the signs of three-step relaxation in other dynamical observables of the confined liquid. Analyzing different dynamical quantities and per-

ceiving the correlations between them lead to a deeper understanding of the surface effects on liquid dynamics. We discuss the wave vector dependence of the scattering function and the temperature dependence of dynamical quantities. Also, we compare the simulation results with analytical calculations for a Fickian liquid in the vicinity of a reflective wall.

We present the results of molecular dynamics simulations of a low molecular weight liquid confined between solid surfaces. The model liquid is hydrogenated methyl methacrylate (HMMA, $C_5H_{10}O_2$) and the model surface is a periodic single layer of pristine graphene which has weak van der Waals interaction with HMMA. The thickness of the confined liquid is around 10 nm. HMMA is similar to the chemical repeating unit of poly(methyl methacrylate), a well-known glass-forming polymer. The selection of HMMA was also motivated by our preliminary work on confined PMMA melts, in which we observed three-step relaxation near the confining surface (data are not shown). Simulations were performed using atomistic models [29, 30]. See section S1 of Supplemental Material for the details.

We analyze the particle displacements perpendicular to the confining surface (i.e., along the z direction), by calculating self-intermediate scattering function ($F_s(q_z, t)$, wave vector is parallel to the z axis), mean-squared displacement ($\langle \Delta z^2(t) \rangle$), second-order non-Gaussian parameter (α_2^z), and self part of the van-Hove function ($G_s(z, t)$) (see section S2 for the definitions). To track the displacements we look at the position of the α -carbon atom of HMMA (see Figure S1). The dynamical quantities are calculated at different distances from the surface (layer-resolved). For the layer-resolved analysis, calcula-

tions are performed on the atoms present in a given layer at $t = 0$.

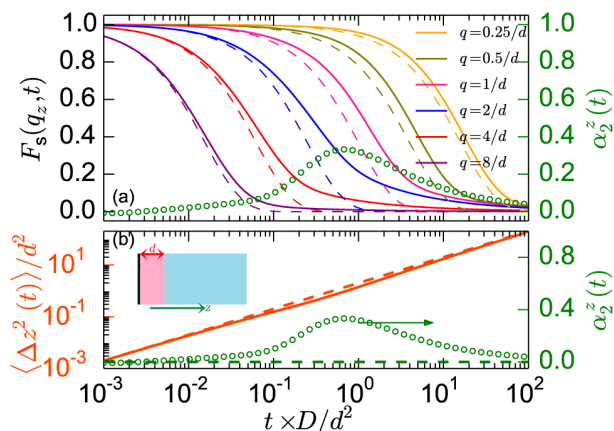


FIG. 1: Solid curves and the curves with the circular marker: the analytically calculated dynamical observables for a layer of Fickian liquid that at $t = 0$ has a thickness of d and is located in contact with a reflective wall (see inset of panel b). The dashed curves display the observables for a bulk Fickian liquid.

Before presenting the simulation results, we examine the above-mentioned dynamical quantities for an idealized case of a liquid that exhibits Fickian diffusion in the vicinity of a reflective wall. Consider a homogeneous layer of the liquid that at $t = 0$ has a thickness of d and is located in contact with a reflective wall (see inset of Figure 1b). This geometry is relevant to the layer-resolved analysis of this work. At the reflective wall $\partial c / \partial z = 0$, where c is the concentration of the particles of the layer. The distribution of displacements, $G_s(z, t)$, for the particles of the tagged layer can be calculated through the reflection of displacements at the wall [31] (see section S3). Using $G_s(z, t)$, different dynamical quantities can be calculated; see Figure 1. The dynamical observables for the particles of the tagged layer deviate from the bulk ones. This is expected because a particle that moves in the negative z direction near the wall has to come back to its original location. The $\alpha_z^z(t)$ of the layer shows a peak. The $F_s(q_z, t)$ of the layer decays slower than the corresponding bulk curve and exhibits a tail; the deviation is pronounced for q_z values around $0.5/d$ to $4/d$. The $\langle \Delta z^2(t) \rangle$ of the layer has an angle around the peak time of $\alpha_z^z(t)$. Around this time, $\langle \Delta z^2(t) \rangle$ first shows a mild sub-diffusive and then a mild super-diffusive behavior. These calculations are useful for understanding the mere geometric effect of confinement on the dynamical observables of the liquid.

In simulations, for the layer-resolved analysis of the dynamics, the confined film is divided into seven layers. Close to the surface, we define six layers of thickness of 4 Å; however, for increasing visibility, we consider the center of the film ([26–50] Å from the surface) as a single

layer (see legends of Figure 2). The selected 4 Å thickness corresponds to the length scale of the local density oscillations (coming from the layered structures of the liquid) close to the surface. Particularly, the first layer corresponds to the first peak of the density profile. At lower temperatures, the layered structure propagates to longer distances (Figure S7).

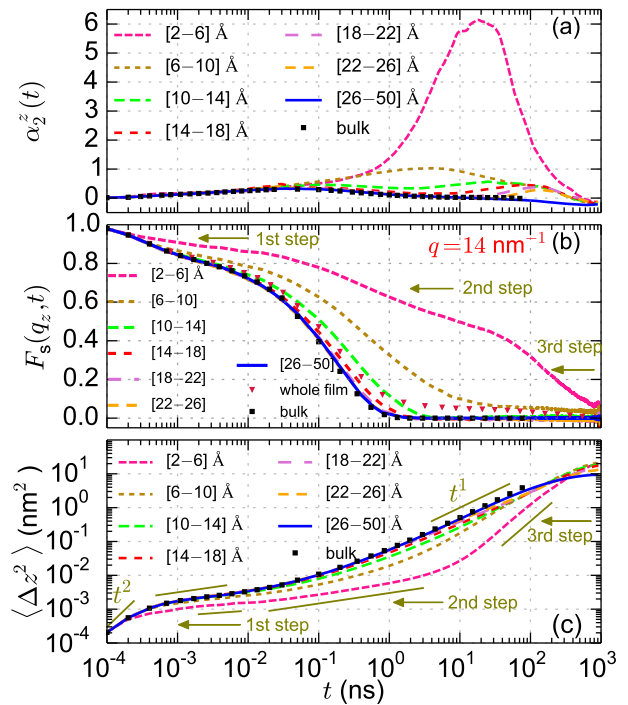


FIG. 2: The layer-resolved $\alpha_z^z(t)$, $F_s(q_z, t)$, and $\langle \Delta z^2(t) \rangle$ curves for characterizing the displacements perpendicular to the surface ($T = 200$ K). In panel (c) the tangent lines show the changes in the slope of the curve.

Figure 2a shows the layer-resolved $\alpha_z^z(t)$ curves at $T = 200$ K, roughly corresponding to $T = 1.4T_g$ (see section S5). The $\alpha_z^z(t)$ of the bulk liquid and of the central layers of the confined liquid exhibit a peak at short times (around 50 ps at 200 K). This peak is related to the dynamical heterogeneity originated from the cage effect (see also Figure S5). The $\alpha_z^z(t)$ of the first layer starts to increase almost in parallel to the bulk $\alpha_z^z(t)$. However, after the peak time of the $\alpha_z^z(t)$ of the bulk liquid, $\alpha_z^z(t)$ of the first layer continues to increase and shows a strong peak at later times. This peak is much stronger than the peak of the $\alpha_z^z(t)$ close to a reflective wall (Figure 1); hence, it is not a mere geometric effect of the confining surface. This strong peak is related to the trapping of the particles in the vicinity of the attractive surface. At short times most of the particles stay in the vicinity of the surface; at intermediate times, some particles escape from the surface but some of them are still trapped near the surface; this leads to heterogeneity of displacements

observed through the peak of $\alpha_2^z(t)$. The $\alpha_2^z(t)$ of the second layer also has a considerable peak, however, it is much lower than that of the first layer. Further, at long times (20 – 200 ns in Figure 2a) small peaks are observed in the $\alpha_2^z(t)$ of the third to sixth layers. The particles belonging to these layers are far from the surface at $t = 0$; after some time, some of those come close to the surface and feel its effects.

Figure 2b shows the layer-resolved $F_s(q_z, t)$ functions at $T = 200$ K at $q_z = 14 \text{ nm}^{-1}$, which is close to the peak position of the structure factor of the α -carbon atoms of HMMA (Figure S4). The $F_s(q_z, t)$ of the bulk liquid and of the central layers shows its typical behavior for a glass-forming liquid at a rather high temperature [19]; it shows a two-step decay, however, the temperature is not low enough to see the full separation between the two steps. At $T = 200$ K, the surface modifies the $F_s(q_z, t)$ of the four adjacent layers. With reducing temperature, the effect of the surface on the liquid dynamics propagates to longer distances. For example at $T = 280$ K, only the first and second layers are affected (see section S7).

The $F_s(q_z, t)$ of the first layer decays slower than that of the bulk liquid. Furthermore, it exhibits a three-step decay (Figure 2b). Similar to the bulk liquid, the first step of the $F_s(q_z, t)$ of the first layer is related to the rattling of the particles in the cages formed by their neighbors. However, the decay of the $F_s(q_z, t)$ of the first layer in its first step is smaller than the decay of the bulk relaxation function in the corresponding step. This behavior probably comes from the modification of the intermolecular packing close to the surface (i.e., the layered structure of the liquid). After cage breaking the particles start cooperative motion; however, because of the attraction of the surface, the particles only have small scale back and forth movements close to the surface. This is reflected in the partial decay of $F_s(q_z, t)$ in its second step. At later times, when the particles start to escape from the surface, an additional relaxation step (the third step) emerges in their $F_s(q_z, t)$. The onset of the third step corresponds to the position of the large peak of the $\alpha_2^z(t)$ of the first layer. (see Figure 3a). For the bulk liquid, the onset of the second step of $F_s(q, t)$ also coincides with the peak of the bulk $\alpha_2(t)$ (see Figure S5). Figure 2b shows also $F_s(q_z, t)$ for the whole confined liquid. This quantity can be measured experimentally, e.g., through quasi-elastic neutron scattering [11]. Note that $F_s^{\text{whole}}(q_z, t) = \sum \phi_i F_{s_i}(q_z, t)$, where ϕ_i and $F_{s_i}(q_z, t)$ are the fraction of the particles present in layer i and its scattering function.

Figure 3a shows the q -dependence of the $F_s(q_z, t)$ of the first layer. In a rather wide range of q , $F_s(q_z, t)$ vanishes at a q -independent time, after the peak time of $\alpha_2^z(t)$. Such a q -dependence resembles the behavior of the single-chain scattering function of entangled polymer melts, which according to the tube model is governed by two processes: chain reptation inside the tube and

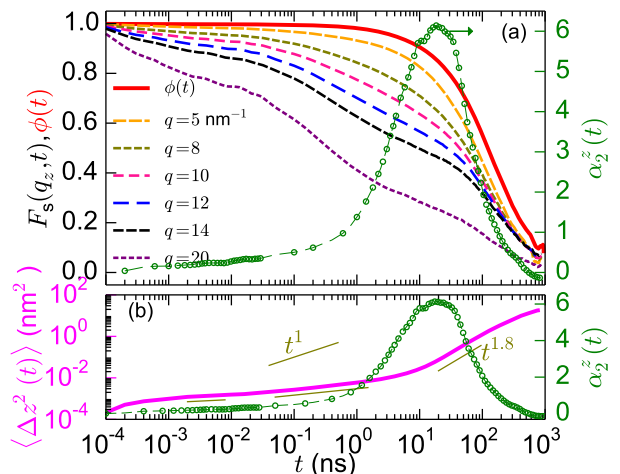


FIG. 3: $F_s(q_z, t)$ and $\langle \Delta z^2(t) \rangle$ of the first layer together with its $\alpha_2^z(t)$. $\phi(t)$ in panel (a) is the fraction of the trapped particles at $t = 0$ which are still trapped (near the same surface) at time t ($T = 200$ K).

the escape of the chain from its confining tube[32]. To understand this q -dependence, we follow the arguments made in [32]. A particle contributes to $F_s(q_z, t)$, if its displacement $\Delta z(t) \lesssim q_z^{-1}$ (i.e., it is slow). The particles which escape from the surface become mobile and, if q_z is not very small, translate by distances larger than q_z^{-1} while some other particles are still trapped near the surface. These mobile particles do not contribute to the scattering function of the first layer and $F_s(q_z, t)$ is dominated by the particles which are still trapped near the surface. Based on this argument, for a range of q_z , the long-time behavior of $F_s(q_z, t)$ of the first layer is controlled by $\phi(t)$ which is the fraction of the trapped particles at $t = 0$ which are still trapped there (near the same surface) at time t . We assume that a scattering center is trapped near the surface if it is located in the first layer. Such particles are also described as adsorbed or attached [33, 34]; also since $\phi(t)$ can be calculated like a correlation function [27, 28, 34, 35], it is usually called desorption correlation function. Because of the confinement in a finite volume, $\phi(t)$ does not decay to zero at long times, instead, converges to the fraction of all particles of the liquid which are trapped near one side of the surface (around 0.045 in the current geometry). $\phi(t)$ can be easily scaled to decay to zero at long times[27, 28, 35], however, we do not scale it, because the finiteness of the confinement volume affects also $F_s(q_z, t)$ and $\Delta z^2(t)$ (see below). $\phi(t)$ at 200 K is shown in Figure 3a. The final decay of the $F_s(q_z, t)$ of the first layer over a wide q range is in good agreement with the final decay of $\phi(t)$, which is consistent with the above discussion. The development of the large peak of $\alpha_2^z(t)$ is also in line with the decay of $\phi(t)$. This is consistent with the discussion of Figure 2a regarding the relation of this peak to the

process of escaping from the surface. With decreasing temperature, the long-time overlap of the $F_s(q_z, t)$ curves (over a range q) becomes more pronounced (see Figure S9). This stems from the higher heterogeneity of particle displacements at lower temperatures (see Figure 4a). With increasing dynamic heterogeneity, the distribution of particle displacements becomes more consistent with the categorization of the particles as trapped (near the surface) and mobile, which is the basis of the argument for the long-time overlap of $F_s(q_z, t)$ (see Figure S10 for the distribution of displacements).

Figure 2c shows the layer-resolved $\langle \Delta z^2(t) \rangle$ curves. Because of confinement in a finite volume, at long times, the $\langle \Delta z^2(t) \rangle$ curves of all layers become constant. After the short-time ballistic regime ($\langle \Delta z^2(t) \rangle \propto t^2$) the $\langle \Delta z^2(t) \rangle$ of the bulk liquid (and of the central layers) exhibits a sub-diffusive regime and then converges to normal diffusion ($\langle \Delta z^2(t) \rangle \propto t^1$). This sub-diffusive regime is related to the cage effect, however, at the studied temperature, 200 K, the cages are not rigid enough to see a plateau [19]. After the ballistic regime, the $\langle \Delta z^2(t) \rangle$ of the first layer shows two sub-diffusive regimes (with different slopes). Similar to the bulk liquid, the first sub-diffusive regime comes from the cage effect. The second regime comes from the trapping effect of the surface; this regime corresponds to the second step of the decay of $F_s(q_z, t)$. After these sub-diffusive regimes, $\langle \Delta z^2(t) \rangle$ increases rapidly and shows a pronounced super-diffusive behavior. The onset of the super-diffusive regime almost concurs with the position of the peak of $\alpha_2^z(t)$, the onset of the third step of $F_s(q_z, t)$, and the onset of the decay of $\phi(t)$ (see Figure 3). This regime is related to the process of escaping from the surface. As shown in Figure 1b, a super-diffusive behavior is also observed close to a reflective wall. However, the effect is much stronger for the model system. To explain the super-diffusive behavior, recall that for the calculation of $\langle \Delta z^2(t) \rangle$ of the first layer, particles that are present in the first layer at $t = 0$ are taken into account. When some of the particles escape from the surface, they finally have diffusive behavior (see $\langle \Delta z^2(t) \rangle$ of the central layers); however, $\langle \Delta z^2(t) \rangle$ calculated relative to the initial positions of the particles in the vicinity of the surface, increases rapidly, and exhibits an apparent super-diffusive behavior. Note that $\langle \Delta z^2(t) \rangle$ is dominated by the fast particles.

Figure 4 shows the temperature dependence of the dynamical observables of the first layer. The presented temperature range approximately corresponds to $2.45T_g$ to $1.26T_g$. The $\alpha_2^z(t)$ curve (panel a) increases at short times because of the heterogeneity originated from the cage effect and later, shows a strong peak because of the surface effect on the displacement of particles. With decreasing temperature, the heterogeneity of the particle displacements significantly increases, reflected in the higher peaks of the $\alpha_2^z(t)$. The distribution of displacements at the peak time of $\alpha_2^z(t)$ is shown in Figure S10.

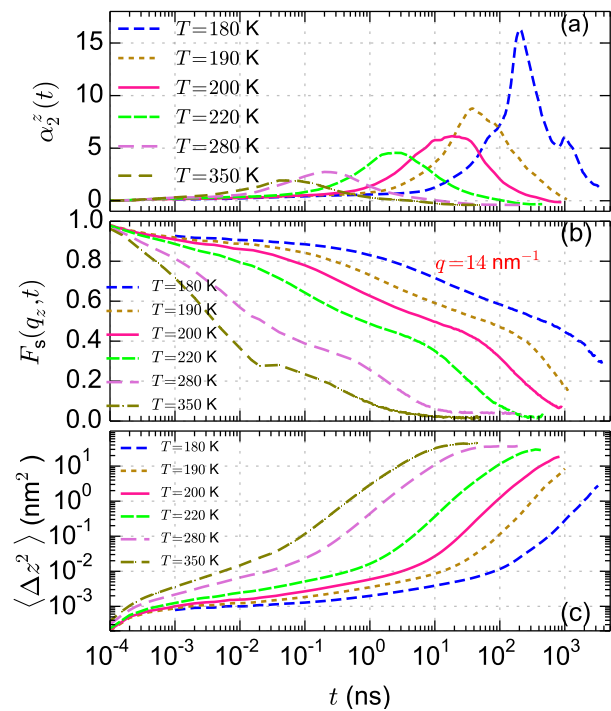


FIG. 4: Temperature dependence of different dynamical quantities for the particles present in the first layer at time origin.

Figure 4b shows the $F_s(q_z, t)$ of the first layer at different temperatures. At high temperatures, the cages are not rigid and their effect is not clearly seen (i.e., at short times $F_s(q_z, t)$ does not have two distinct steps). As for bulk glass-forming liquids, upon reducing temperature, the time scales of the first and second steps of $F_s(q_z, t)$ become more separated. This is reflected in the appearance of an extended plateau between the first and second steps. With reducing temperature, such a sign of time scale separation between the second and the third steps of $F_s(q_z, t)$ of the first layer is not observed; on the contrary, the separation between the second and third steps becomes less clear and their time scales seem to come closer to each other. Furthermore, the contribution of the third step in the decay of $F_s(q_z, t)$ seems to increase; that is, the onset of the third step appears at larger F_s values. The $F_s(q_z, t)$ curves have also been analyzed by fitting their second and third steps with the sum of two stretched-exponential functions (see section S10). The time scales of these steps have been estimated from the fitted functions and they are in favor of the gradual merging of the second and third steps with decreasing temperature. The merging can be explained as follows: At low temperatures the particles face large (caging or packing) barriers for their motions; if some of the particles can overcome these barriers, they probably can also overcome the energetic barriers for escaping from the surface. Long-time tails are also observed after the third

step of $F_s(q_z, t)$. The appearance of this tail almost concurs with the convergence of $\langle \Delta z^2(t) \rangle$ to a constant value and it is related to the confinement of the liquid in a finite volume.

Figure 4c shows the $\langle \Delta z^2(t) \rangle$ of the first layer at different temperatures. At low temperatures, two sub-diffusive regimes can be detected (which are discussed above). At high temperatures, the cages are not rigid enough and their restricting effects are not seen; hence only one sub-diffusive regime is observed. Furthermore, at lower temperatures, transition to the super-diffusive regime occurs at smaller $\langle \Delta z^2(t) \rangle$ values. This is consistent with the smaller contribution of the second step in the decay of $F_s(q_z, t)$ at lower temperatures. With decreasing temperature, the slope of the second sub-diffusive regime gradually reduces and the slope of the super-diffusive regime seems to gradually increase.

In summary, we analyzed the displacements of the particles of a liquid perpendicular to an attractive confining surface. The surface imposes a large heterogeneity on the displacements in the adjacent liquid and also leads to its three-step relaxation. The first step is related to the rattling of particles in the cages; the second step is related to the small-scale movements close to the surface, and the third step is related to the process of escaping from the surface. With decreasing temperature, the surface-induced dynamical heterogeneity increases, and the second and third relaxation steps seem to be gradually combined.

* aforooza@uni-mainz.de

- [1] Peter Scheidler, Walter Kob, and Kurt Binder, “Cooperative motion and growing length scales in supercooled confined liquids,” *Europhys. Lett.* **59**, 701 (2002).
- [2] Peter Scheidler, Walter Kob, and Kurt Binder, “The relaxation dynamics of a supercooled liquid confined by rough walls,” *J. Phys. Chem. B* **108**, 6673–6686 (2004).
- [3] JA Torres, PF Nealey, and JJ De Pablo, “Molecular simulation of ultrathin polymeric films near the glass transition,” *Physical Review Letters* **85**, 3221 (2000).
- [4] Grant D Smith, Dmitry Bedrov, and Oleg Borodin, “Structural relaxation and dynamic heterogeneity in a polymer melt at attractive surfaces,” *Phys. Rev. Lett.* **90**, 226103 (2003).
- [5] Jean-Louis Barrat, Jörg Baschnagel, and Alexey Lyulin, “Molecular dynamics simulations of glassy polymers,” *Soft Matter* **6**, 3430–3446 (2010).
- [6] Walter Kob, Sándalo Roldán-Vargas, and Ludovic Berthier, “Non-monotonic temperature evolution of dynamic correlations in glass-forming liquids,” *Nat. Phys.* **8**, 164–167 (2012).
- [7] Raffaele Pastore and Guido Raos, “Glassy dynamics of a polymer monolayer on a heterogeneous disordered substrate,” *Soft matter* **11**, 8083–8091 (2015).
- [8] Wengang Zhang, Jack F Douglas, and Francis W Starr, “Why we need to look beyond the glass transition temperature to characterize the dynamics of thin supported polymer films,” *Proc. Natl. Acad. Sci. U.S.A.* **115**, 5641–5646 (2018).
- [9] Robin Horstmann, Lukas Hecht, Sebastian Kloth, and Michael Vogel, “Structural and dynamical properties of liquids in confinements: A review of molecular dynamics simulation studies,” *Langmuir* **38**, 6506–6522 (2022).
- [10] M Arndt, R Stannarius, H Grootshues, E Hempel, and F Kremer, “Length scale of cooperativity in the dynamic glass transition,” *Phys. Rev. Lett.* **79**, 2077 (1997).
- [11] Margarita Krutyeva, Jaime Martin, Arantxa Arbe, Juan Colmenero, Carmen Mijangos, Gerald J Schneider, Tobias Unruh, Yixi Su, and Dieter Richter, “Neutron scattering study of the dynamics of a polymer melt under nanoscopic confinement,” *J. Chem. Phys.* **131**, 174901 (2009).
- [12] Aurélie Papon, Hélène Montes, Mohamed Hanafi, François Lequeux, Laurent Guy, and Kay Saalwächter, “Glass-transition temperature gradient in nanocomposites: evidence from nuclear magnetic resonance and differential scanning calorimetry,” *Phys. Rev. Lett.* **108**, 065702 (2012).
- [13] Anna Panagopoulou, Cristian Rodríguez-Tinoco, Ronald P White, Jane EG Lipson, and Simone Napolitano, “Substrate roughness speeds up segmental dynamics of thin polymer films,” *Phys. Rev. Lett.* **124**, 027802 (2020).
- [14] Shiwang Cheng and Alexei P Sokolov, “Correlation between the temperature evolution of the interfacial region and the growing dynamic cooperativity length scale,” *J. Chem. Phys.* **152**, 094904 (2020).
- [15] Melanie Reuhl, Philipp Monnard, and Michael Vogel, “Confinement effects on glass-forming mixtures: Insights from a combined experimental approach to aqueous ethylene glycol solutions in silica pores,” *J. Chem. Phys.* **156**, 084506 (2022).
- [16] MD Ediger and JA Forrest, “Dynamics near free surfaces and the glass transition in thin polymer films: a view to the future,” *Macromolecules* **47**, 471–478 (2014).
- [17] Kenneth S Schweizer and David S Simmons, “Progress towards a phenomenological picture and theoretical understanding of glassy dynamics and vitrification near interfaces and under nanoconfinement,” *J. Chem. Phys.* **151**, 240901 (2019).
- [18] Wolfgang Götze, *Complex dynamics of glass-forming liquids: A mode-coupling theory*, Vol. 143 (Oxford University Press on Demand, 2009).
- [19] Kurt Binder and Walter Kob, *Glassy materials and disordered solids: An introduction to their statistical mechanics* (World scientific, 2011).
- [20] Raffaele Pastore, Antonio Coniglio, and Massimo Pica Ciamarra, “From cage-jump motion to macroscopic diffusion in supercooled liquids,” *Soft Matter* **10**, 5724–5728 (2014).
- [21] J Helfferich, F Ziebert, S Frey, H Meyer, J Farago, A Blumen, and J Baschnagel, “Continuous-time random-walk approach to supercooled liquids. i. different definitions of particle jumps and their consequences,” *Physical Review E* **89**, 042603 (2014).
- [22] Walter Kob, Claudio Donati, Steven J Plimpton, Peter H Poole, and Sharon C Glotzer, “Dynamical heterogeneities in a supercooled lennard-jones liquid,” *Phys. Rev. Lett.* **79**, 2827 (1997).
- [23] David R Reichman and Patrick Charbonneau, “Mode-

- coupling theory,” *J. Stat. Mech.: Theory Exp.* **2005**, P05013 (2005).
- [24] Bart Vorselaars, Alexey V Lyulin, K Karatasos, and MAJ Michels, “Non-gaussian nature of glassy dynamics by cage to cage motion,” *Phys. Rev. E* **75**, 011504 (2007).
- [25] S Peter, H Meyer, and J Baschnagel, “Md simulation of concentrated polymer solutions: Structural relaxation near the glass transition,” *Eur. Phys. J. E* **28**, 147–158 (2009).
- [26] Ludovic Berthier and Giulio Biroli, “Theoretical perspective on the glass transition and amorphous materials,” *Rev. Mod. Phys.* **83**, 587 (2011).
- [27] L Yelash, P Virnau, K Binder, and W Paul, “Three-step decay of time correlations at polymer-solid interfaces,” *EPL (Europhys. Lett.)* **98**, 28006 (2012).
- [28] M Solar, K Binder, and W Paul, “Relaxation processes and glass transition of confined polymer melts: A molecular dynamics simulation of 1, 4-polybutadiene between graphite walls,” *J. Chem. Phys.* **146**, 203308 (2017).
- [29] Alireza F Behbahani, G Hashemi Motlagh, S Mehdi Vaez Allaei, and Vagelis A Harmandaris, “Structure and conformation of stereoregular poly (methyl methacrylate) chains adsorbed on graphene oxide and reduced graphene oxide via atomistic simulations,” *Macromolecules* **52**, 3825–3838 (2019).
- [30] Alireza Foroozani Behbahani and Vagelis Harmandaris, “Gradient of segmental dynamics in stereoregular poly (methyl methacrylate) melts confined between pristine or oxidized graphene sheets,” *Polymers* **13**, 830 (2021).
- [31] John Crank, *The mathematics of diffusion* (Oxford university press, 1979).
- [32] PG De Gennes, “Coherent scattering by one reptating chain,” *J. Phys.* **42**, 735–740 (1981).
- [33] Kurt A Smith, Mihail Vladkov, and Jean-Louis Barrat, “Polymer melt near a solid surface: A molecular dynamics study of chain conformations and desorption dynamics,” *Macromolecules* **38**, 571–580 (2005).
- [34] Alireza F Behbahani, Anastassia Rissanou, Giorgos Kritikos, Manolis Doxastakis, Craig Burkhart, Patrycja Polińska, and Vagelis A Harmandaris, “Conformations and dynamics of polymer chains in cis and trans polybutadiene/silica nanocomposites through atomistic simulations: From the unentangled to the entangled regime,” *Macromolecules* **53**, 6173–6189 (2020).
- [35] L Yelash, P Virnau, K Binder, and W Paul, “Slow process in confined polymer melts: Layer exchange dynamics at a polymer solid interface,” *Phys. Rev. E* **82**, 050801 (2010).

Supplemental Material: Relaxation Dynamics of a Liquid in the Vicinity of an Attractive Surface: The Process of Escaping from the Surface

Alireza F. Behbahani^{1,2,*} and Vagelis Harmandaris^{3,2,4}

¹*Institut für Physik, Johannes Gutenberg-Universität Mainz,
Staudingerweg 7, D-55099 Mainz, Germany*

²*Institute of Applied and Computational Mathematics,
Foundation for Research and Technology - Hellas, Heraklion GR-71110, Greece*

³*Computation-based Science and Technology Research Center,
The Cyprus Institute, Nicosia 2121, Cyprus*

⁴*Department of Mathematics and Applied Mathematics,
University of Crete, Heraklion GR-71110, Greece*

(Dated: July 4, 2023)

S1. MODEL AND METHOD

Figure S1a shows the studied model geometry. In this figure, the simulation box together with one of its periodic images (along the z direction) is presented. Figure S1b shows a schematic representation of the chemical structure of the model studied liquid, hydrogenated methyl methacrylate (HMMA). The confining surface is a periodic single-layer of pristine graphene. The graphen surface is not frozen, i.e., the equations of motion for the wall particles are also taken into account. The surface was placed parallel to the xy plane and periodic boundary condition was applied along all directions. At 200 K, the dimensions of the simulation box are almost $5.2 \times 5.2 \times 10.3 \text{ nm}^3$ along the x , y , and z directions. The periodic boundary conditions make the model geometry a multi-layered system containing alternating almost 10 nm thick films of HMMA confined between infinite surfaces. We performed molecular dynamics simulations with atomistic models using the GRO-MACS package [1]. The leap-frog algorithm with 1 fs time step was used for the integration of the equations of motion. Simulations were performed at constant temperature and constant pressure (NPT ensemble). Nosé-Hoover thermostat with 0.5 ps relaxation time and Parrinello-Rahman barostat with 5 ps relaxation time (for anisotropic pressure coupling) were used for controlling temperature and pressure. Depending on the temperature, we performed simulations for 100 ns up to more than 4 μs . The nonbonded interactions were truncated at 1 nm. Van der Waals tail

* aforooza@uni-mainz.de

correction was applied to energy and pressure and the particle-mesh Ewald method was employed for the calculation of the long-range electrostatic interactions. The Lorentz-Berthelot mixing rule was used for the calculation of the interactions between dissimilar atoms. The carbon atoms of graphene have weak attractive van der Waals interactions (modeled with the Lennard-Jones pair potential) with the atoms of HMMA. In the employed model, the depth of the individual Lennard-Jones interactions between the carbon atoms of graphene and carbon atoms of HMMA is around 0.33 kJ/mol which is slightly smaller than the interaction energy between two carbon atoms of HMMA. However, each atom of HMMA interacts with several carbon atoms of graphene, which have a packed honeycomb structure with a bond length of around 1.42 Å. Figure S1c shows a relaxed configuration of a single HMMA molecule on the graphene surface (the separation of this configuration from graphene cots around 47 kJ/mol). The van der Waals interactions between the graphene surface and the HMMA liquid lead to the layered structure of the liquid in the vicinity of the surface (see Figure S7). The details of the employed force field can be found elsewhere [2].

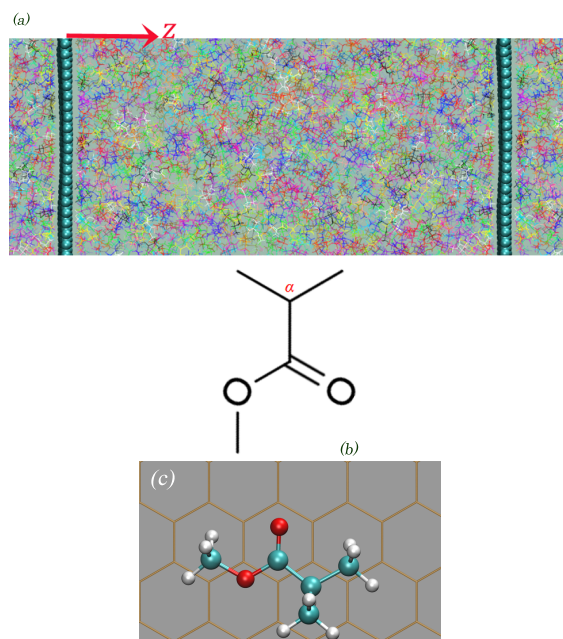


FIG. S1: (a) The studied geometry. A snapshot of the simulation box and one of its period images along the z direction are shown. (b) A schematic representation of the chemical structure of HMMA. α -carbon atom of HMMA is also shown. (c) Top view of a relaxed configuration of one HMMA molecule on the graphene surface.

S2. THE DEFINITIONS OF THE STUDIED DYNAMICAL QUANTITIES

In the confined liquid, the displacements of particles perpendicular to the surface (along the z direction) are analyzed by calculating self intermediate scattering function ($F_s(q_z, t)$, wave vector is parallel to the z axis), mean-squared displacement ($\langle \Delta z^2(t) \rangle$), second-order non-Gaussian parameter (α_2^z), and self part of the van-Hove function ($G_s(z, t)$) defined as :

$$\begin{aligned}
 F_s(q_z, t) &= \langle \cos[q_z \Delta z(t)] \rangle \\
 \langle \Delta z^2(t) \rangle &= \langle (z(t) - z(0))^2 \rangle \\
 \alpha_2^z(t) &= \frac{1}{3} \frac{\langle \Delta z^4 \rangle}{\langle \Delta z^2 \rangle^2} - 1 \\
 G_s(z, t) &= \langle \delta(z - [z_i(t) - z_i(0)]) \rangle
 \end{aligned} \tag{S1}$$

where $\langle \rangle$ shows averaging over appropriate atoms and time origins and δ is the delta function. For the isotropic bulk liquid, the dynamical properties along all different directions are identical and the following relations can also be used:

$$\begin{aligned}
 F_s(q, t) &= \left\langle \frac{\sin[q \Delta r(t)]}{q \Delta r(t)} \right\rangle \\
 \text{MSD}(t) &= \langle \Delta r^2(t) \rangle = \langle (r(t) - r(0))^2 \rangle \\
 \alpha_2(t) &= \frac{3}{5} \frac{\langle \Delta r^4 \rangle}{\langle \Delta r^2 \rangle^2} - 1
 \end{aligned} \tag{S2}$$

where $\text{MSD}(t)$ is the total mean-squared displacement of particles which in the case of isotropic systems is equal to $3\langle \Delta z^2(t) \rangle$.

S3. DYNAMICAL OBSERVABLES FOR A FICKIAN LIQUID CLOSE TO A REFLECTIVE WALL

In a bulk liquid, if the particles have Fickian diffusion then the distribution of their displacements is Gaussian: $G_s(z, t) = \exp(-z^2/4Dt)/\sqrt{4\pi Dt}$, $\alpha_2^z(t) = 0$, $\langle \Delta z^2(t) \rangle = 2Dt$, and $F_s(q_z, t) = \exp(-q_z^2 Dt)$, where D is the diffusion coefficient of the particles the liquid. Now, consider some tagged particles of a Fickian liquid that at $t = 0$ are located at a distance z_0 from an ideal planar reflective wall (that is, at $t = 0$ the spatial distribution of particles is $\delta(z - z_0)$, see the inset of [Figure S2b](#)). At the reflective wall $\partial c / \partial z = 0$, where c is the concentration of the tagged particles. The distribution of displacements of the tagged particles (displacements relative to the position at $t = 0$) can be calculated via reflection of the displacements at the wall. For these tagged

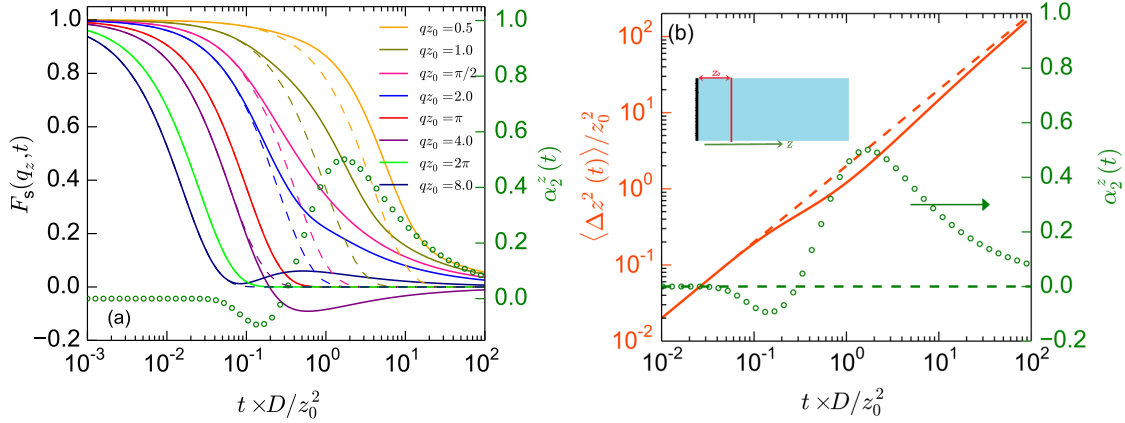


FIG. S2: Solid curves and the curves with circle marker: the analytically calculated dynamical observables for some tagged particles of a Fickian liquid that at $t = 0$ are located at distance z_0 from a reflective wall (see inset of panel b). The dashed curves display the observables for a bulk liquid with Fickian diffusion of particles.

particles: $G_s(z, t) = [\exp(-z^2/4Dt) + \exp(-(z + 2z_0)^2/4Dt)]/\sqrt{4\pi Dt}$, $z \geq -z_0$. With $G_s(z, t)$ at hand $F_s(q_z, t)$, $\langle \Delta z^2(t) \rangle$, and $\alpha_2^z(t) = 0$ can be calculated:

$$\begin{aligned}
 F_s(q_z, t) &= \int_{-\infty}^{\infty} G_s(z, t) \cos[q_z z] dz \\
 \langle \Delta z^2(t) \rangle &= \int_{-\infty}^{\infty} G_s(z, t) z^2 dz \\
 \langle \Delta z^4(t) \rangle &= \int_{-\infty}^{\infty} G_s(z, t) z^4 dz \\
 \alpha_2^z(t) &= \frac{1}{3} \frac{\langle \Delta z^4 \rangle}{\langle \Delta z^2 \rangle^2} - 1
 \end{aligned} \tag{S3}$$

We calculated the above integrals numerically. The results are presented in [Figure S2](#). The geometric effect of the wall modifies the dynamical observables of the tagged particles. The behavior of $F_s(q_z, t)$ is interesting. Generally the $F_s(q_z, t)$ curves of the tagged particles differ from the bulk curves. However, at $q = n\pi/z_0$ ($n = 1, 2, 3, \dots$), the $F_s(q_z, t)$ of the tagged particles are similar to the bulk ones. Furthermore, at some q values (e.g., $q = 4/z_0$ and $q = 8/z_0$ in [Figure S2](#)), the $F_s(q_z, t)$ curves are non-monotonic. For example, at $q = 4/z_0$, $F_s(q_z, t)$ becomes negative before converging to zero; or at $q = 8/z_0$, $F_s(q_z, t)$ becomes almost zero and then increases again. Such non-monotonic shapes can also be observed in the simulations through layer-resolved calculations of $F_s(q_z, t)$ for very thin layers. For example see [Figure S3](#).

Now, we consider a homogeneous layer of tagged particles that at $t = 0$ has a finite thickness of d and is located in contact with a reflective wall (see inset of [Figure 1b](#) of the main article). For

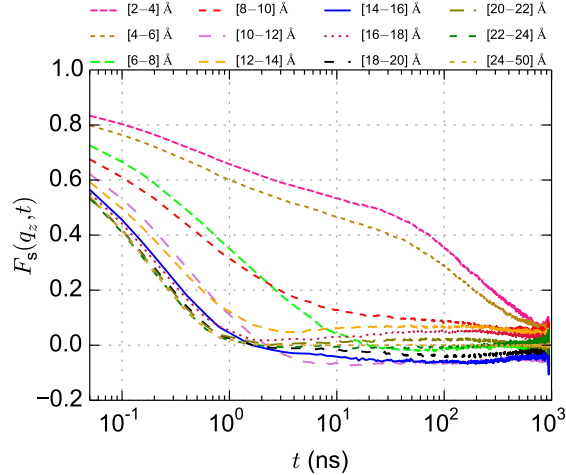


FIG. S3: $F_s(q, t)$ curves calculated for thin 2 Å layers in the confined liquid ($T = 200$ K). The $F_s(q, t)$ curves of some of the layers show a non-monotonic behavior which is consistent with the analytical results presented in Figure S2.

these tagged particles the distribution of displacements can be calculated through:

$$G_s(z, t) = \frac{1}{d\sqrt{4\pi Dt}} \int_0^d [\exp(-z^2/4Dt) + \exp(-(z + 2z_0)^2/4Dt)] H(z + z_0) dz_0 \quad (\text{S4})$$

where $H(\cdot)$ is the unit (Heaviside) step function ($H(x) = 1$ for $x \geq 0$ and $H(x) = 0$ for $x < 0$). The above integral was also calculated numerically. The calculated dynamical observables using the above relation for $G_s(z, t)$ are provided in Figure 1 of the main article.

S4. STRUCTURE FACTORS OF THE BULK LIQUID

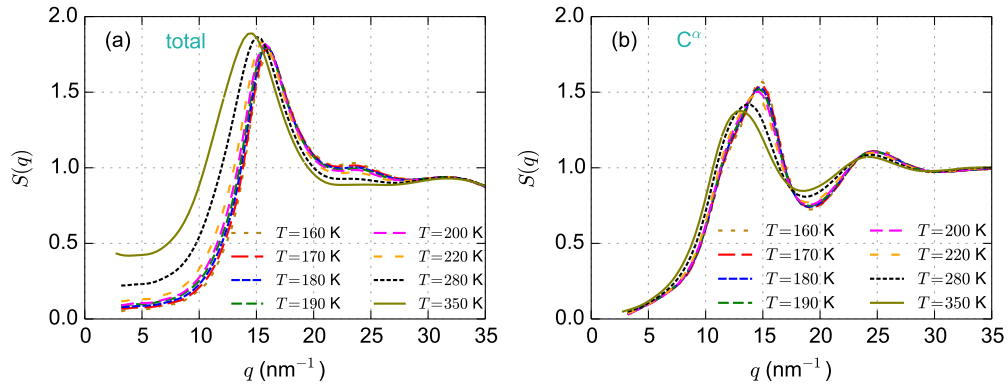


FIG. S4: (a) Static structure factor of the HMMA liquid at different temperatures. (b) Partial structure factor of the α -carbon atoms of HMMA at different temperatures.

The static structure factors of the model liquid, at different temperatures, are shown in [Figure S4a](#). [Figure S4b](#) shows the partial structure factor of the α -carbon atoms of HMMA. With reducing temperature, the peak of $S(q)$ shifts to slightly larger q values. This is the result of the increasing density of the liquid with decreasing temperature. The $F_s(q, t)$ curves are mainly calculated at $q = 14 \text{ nm}^{-1}$ which is close to the peak position of the partial structure factor of the α -carbon atoms. Note that the experimental melting point of HMMA is 188 K [3]. However, in the simulation of the model HMMA liquid, we do not see any sign of crystallization or a time-dependent behavior at temperatures lower than 188 K. This observation originates from the much longer time scales of crystallization than the simulation time window. Furthermore, the melting temperature of the model HMMA liquid might deviate from that of the experimental sample (due to the choice of the force field).

S5. DYNAMICS OF THE BULK LIQUID

The dynamical observables for the bulk HMMA liquid at various temperatures are shown in [Figure S5](#). Upon reducing temperature, dynamical heterogeneities related to the cage effect increases. This is reflected in the higher peaks of $\alpha_2(t)$ at lower temperatures ([Figure S5a](#)). Furthermore, at lower temperatures, the cages are more rigid. This is reflected in the development of plateau regimes in the $F_s(q, t)$ and $\text{MSD}(t)$ curves ([Figure S5b-c](#)). The maximum of $\alpha_2(t)$ almost coincides with the onset of decay of $F_s(q, t)$ and also onset of increase of $\text{MSD}(t)$, after the cage regime.

From the $F_s(q, t)$ curves we can calculate the relaxation times of the α -process in the liquid. We fitted an stretched exponential function ($f(t) = A \exp(-(t/\tau)^\beta)$) on each $F_s(q, t)$ curve and calculated the relaxation times through $\tau_c = \tau/\beta\Gamma(1/\beta)$, where Γ is the Gamma function. The calculated relaxation times at different temperatures are presented in [Figure S6](#). To describe the temperature dependence of α -relaxation, we fitted a Vogel-Fulcher-Tammann (VFT) function ($\tau_c = \tau_\infty \exp(B/(T - T_0))$) on the relaxation times (see the dashed line in [Figure S6](#)). The fitting parameters are: $T_0 = 129.0 \text{ K}$, $B = 500 \text{ K}$, and $\tau_\infty = 0.00016 \text{ ns}$.

Usually, the T_g of a liquid is measured as the temperature at which the relaxation time of α -relaxation equals around 100 s. This time scale is very far from the accessible time scales of molecular simulations, however, from the fitted VFT relation we can calculate a rough estimate of T_g . Especially for the studied model liquid, a clear deviation from the Arrhenius temperature dependence of the relaxation times is seen in the temperature range of this study and hence the VFT parameters can be determined rather reliably. For the model HMMA liquid, $T_g \approx 143 \text{ K}$ assuming

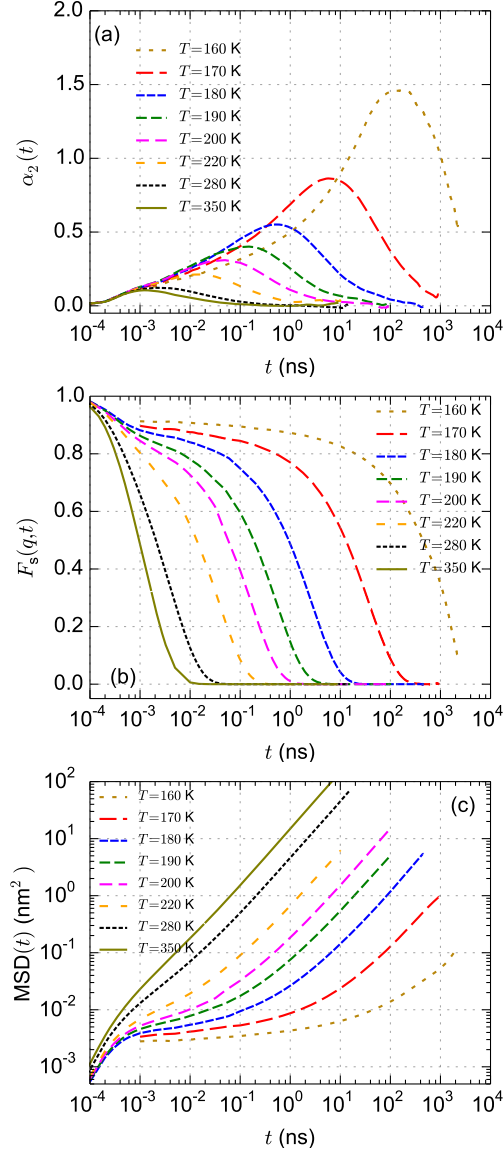


FIG. S5: Dynamical observables for the model liquid at different temperatures. (a), (b), and (c) show non-Gaussian parameter, self-intermediate scattering function, and mean-squared displacement, respectively.

$\tau_c(T_g) = 100$ s. Hence, the temperature range shown in Figure S5, approximately corresponds to $2.45T_g$ down to $1.12T_g$.

S6. INTERFACIAL DENSITY PROFILES

The interfacial mass density profiles for the model confined system are presented in Figure S7. The density profiles are calculated as a function of axial distance (the distance on the z axis) from

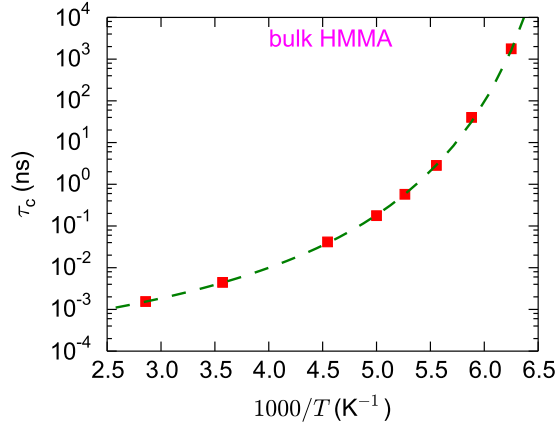


FIG. S6: Temperature dependence of the relaxation times of α -process. The dashed curve is the fitted VFT curve on the data.

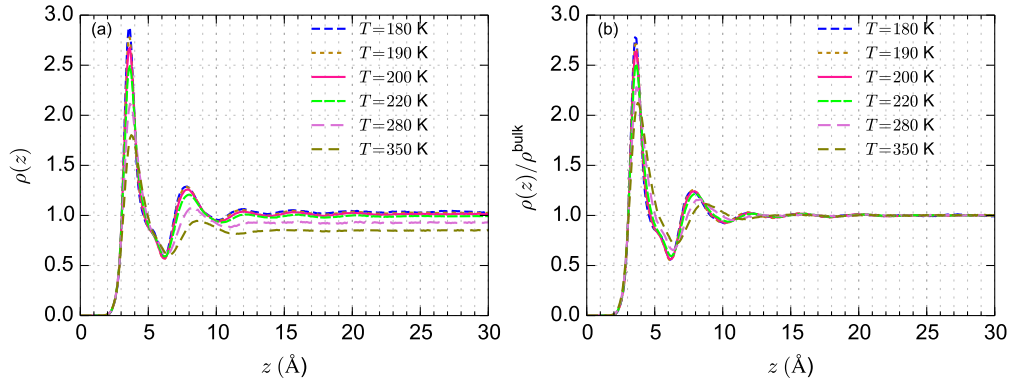


FIG. S7: Interfacial mass density profiles of the confined liquid as a function of axial distance from the center-of-mass of the confining surface. In panel (b) the density profiles are normalized by the respective bulk densities.

the center of mass of the confining surface. For the calculations, the space is divided into thin slabs of 0.05 \AA thickness and the density of the liquid in each slab is calculated. Figure S7a shows the density profiles without normalization and Figure S7b shows the density profiles normalized by the respective bulk values.

S7. THE LAYER-RESOLVED $F_s(q, t)$ CURVES AT DIFFERENT TEMPERATURES

Figure S8 shows the layer-resolved $F_s(q, t)$ functions of the confined liquid at different temperatures (220 K, 280 K, and 180 K). With reducing temperature, the length scale over which the confining surface modifies the dynamics of the liquid increases. At $T = 280 \text{ K}$, the dynamics

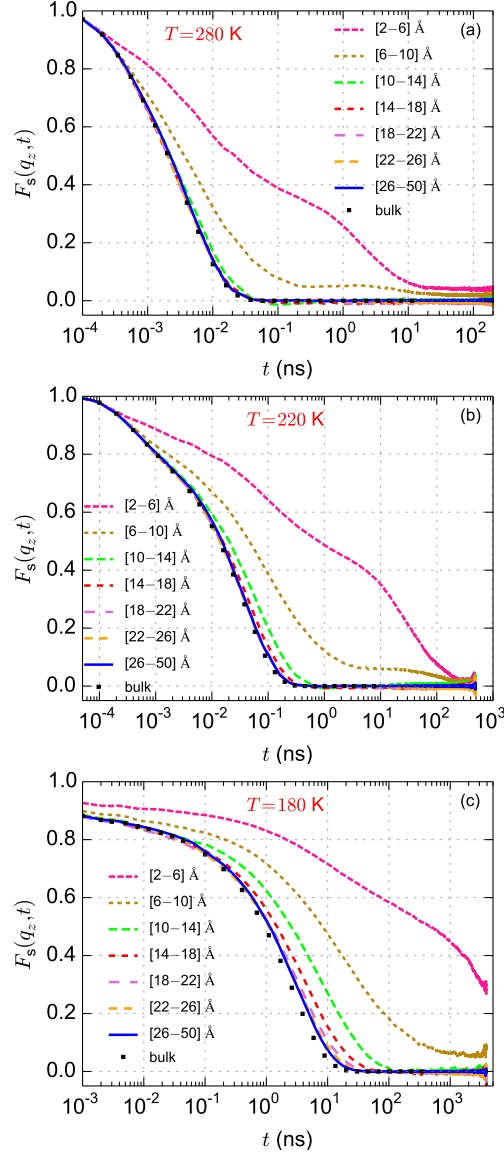


FIG. S8: Layer-resolved $F_s(q, t)$ curves for the confined liquid at (a) $T = 280$ K, (b) $T = 220$ K, and (c) $T = 180$ K ($q = 14 \text{ nm}^{-1}$).

in the first and the second layers are affected by the confining surface. However, with reducing temperature, the dynamics in the further layers are also modified. At $T = 220$ K, the dynamical gradient propagates up to the fourth layer, and at $T = 180$ K, up to the fifth one. This trend correlates with the more pronounced layered structure of the liquid close to the surface at lower temperatures (see Figure S5). It is worth mentioning that the increase of the length scale of the surface effect has also been observed for confined liquids that have a similar structure to the bulk liquid [4]. In these cases the increase of the length scale was explained by increasing the size of cooperatively rearranging regions with decreasing temperature.

S8. THE q -DEPENDENCE OF THE $F_s(q, t)$ OF THE FIRST LAYER AT DIFFERENT TEMPERATURES

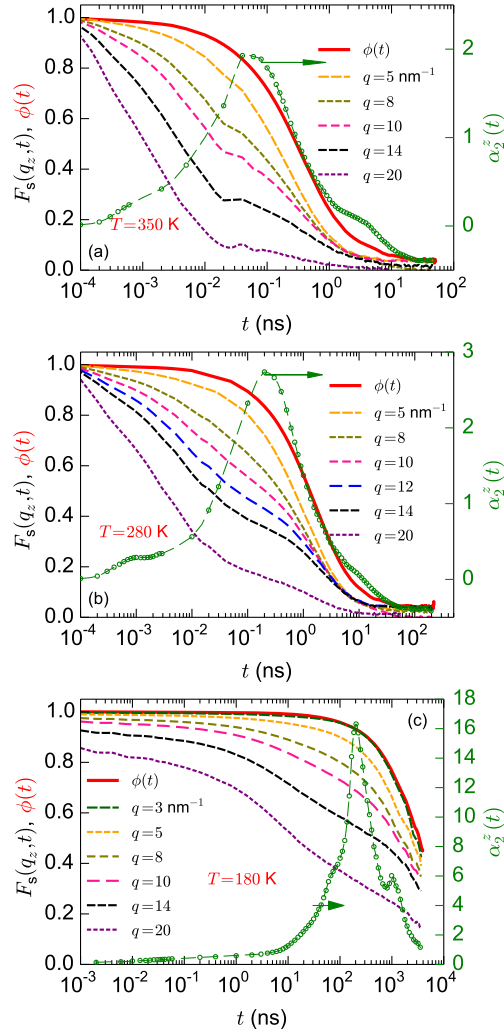


FIG. S9: The q -dependence of the $F_s(q, t)$ of the first layer at (a) $T = 350$ K, (b) $T = 280$ K, and (c) $T = 180$ K. In each panel, $\phi(t)$ and $\alpha_z^2(t)$ of the first layer are also presented. $\phi(t)$ is the fraction of the trapped molecules at $t = 0$ which are still trapped near the surface at time t .

Figure S9 shows the q -dependence of the $F_s(q, t)$ of the first layer at $T = 350$ K, $T = 280$ K, and $T = 180$ K. For a discussion of this figure, see the main text, the discussion of Figure 3a, in which the q -dependence of $F_s(q, t)$ of the first layer at $T = 200$ K is presented.

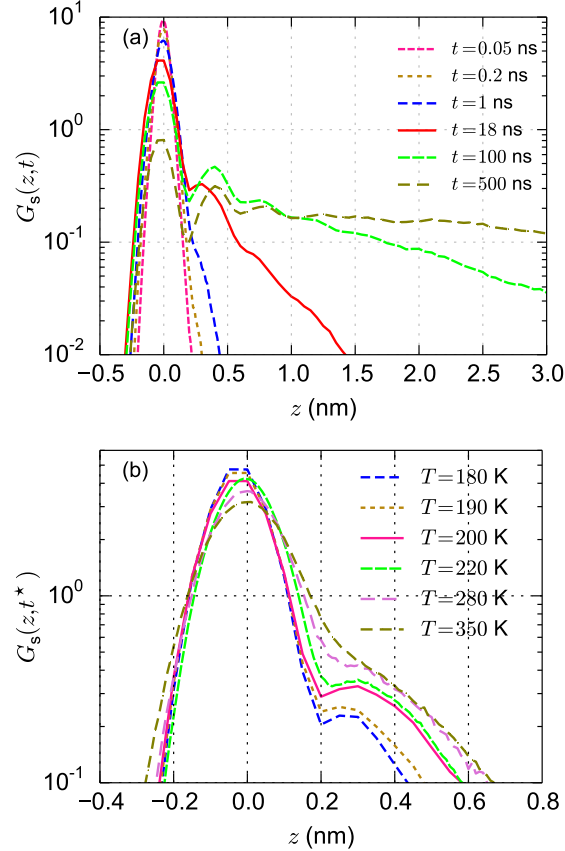


FIG. S10: The self part of the van-Hove function, $G_s(z, t)$, for the particles that are present in the first layer at time origin. (a) $G_s(z, t)$ at $T = 200$ K at different times. Here, $t = 18$ ns (the solid red curve) almost corresponds to the peak time of $\alpha_2^z(t)$. (b) $G_s(z, t^*)$ at different temperatures. t^* is the peak time of $\alpha_2^z(t)$.

S9. THE DISTRIBUTION OF DISPLACEMENTS

Figure S10 shows simulating results for the self part of the van-Hove function, $G_s(z, t)$, for the particles that are present in the first layer ($[2-6]$ Å from the surface) at $t = 0$. $G_s(z, t)$ simply shows the distribution of particle displacements along the z direction. The distribution of displacements for the particles that are located on the right-hand side of the confining surface and the distribution for the particles that are located on the left-hand side are expected to be symmetric under reflection with respect to $z = 0$. Hence, here, the distribution of displacements for the left-hand side particles has been reflected over $z = 0$ and then the average distribution has been calculated. Figure S10a shows the $G_s(z, t)$ at different times at $T = 200$ K. At short times, the particles have small movements within the layer and $G_s(z, t)$ has an almost symmetric shape.

Gradually some particles leave the layer and diffuse toward the center of the film. At later times a secondary peak is seen in $G_s(z, t)$. This secondary peak originates from the layered structure of the liquid close to the surface. The distance between the first and second peaks is similar to the distances between the first and second peaks of the density profile of the α -carbon atoms (the target atoms for the calculation of van-Hove functions). Figure S10b shows $G_s(z, t^*)$ at different temperature. t^* is the peak time of $\alpha_2^z(t)$ (the $\alpha_2^z(t)$ curves are shown in the Figure 4a of the main text). At all temperatures $G_s(z, t^*)$ exhibits a shoulder which is related to the displacement of the particles which have escaped from the surface. With reducing temperature the height of the main peak of $G_s(z, t^*)$ increases. This large peak is related to the displacement of slow particles which are still trapped near the surface. Furthermore, the shoulder of $G_s(z, t^*)$ becomes more pronounced and appears as a small secondary peak

S10. QUANTITATIVE ANALYSIS OF THE $F_s(q, t)$ CURVES OF THE FIRST LAYER

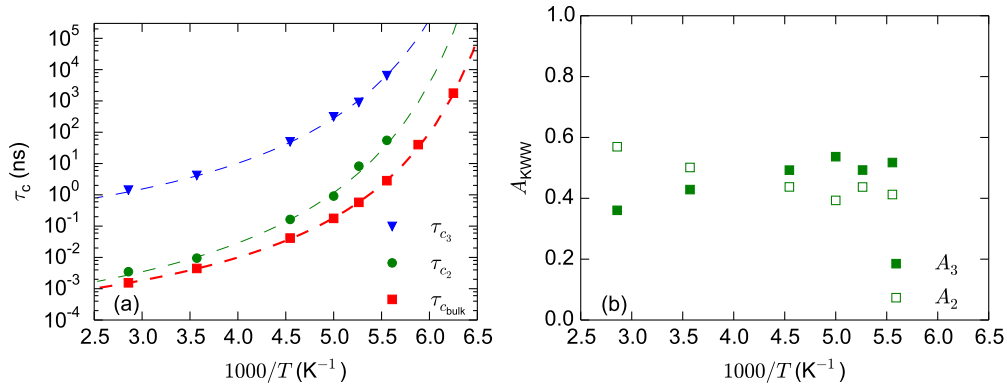


FIG. S11: (a) The estimated relaxation times of the second and third steps of the $F_s(q_z, t)$ of the first layer, [2–6] Å from the surface. (b) The contributions of the second and third steps in the decay of the $F_s(q_z, t)$ of the first layer are estimated by fitting $F_s(q_z, t)$ curves with a sum of two stretched exponential functions. A_2 and A_3 are the weights of the stretched exponential functions.

In this section we analyze the $F_s(q_z, t)$ curves of the first layer of the confined liquid by fitting the second and third steps of F_s with the sum of two stretched-exponential functions: $f(t) = A_2 \exp[-(t/\tau_2)^{\beta_2}] + A_3 \exp[-(t/\tau_3)^{\beta_3}]$ ($A_2 + A_3 < 1$). The mean relaxation time associated with each step has been calculated using $\tau_{c_i} = \tau_i/\beta_i\Gamma(1/\beta_i)$, where Γ is the gamma function. The values τ_{c_i} at different temperatures are provided in Figure S11a. For bulk glass-forming liquids, with reducing temperature α -relaxation becomes more separated from the process of movements

in the cages. As shown in [Figure S11a](#), the second and third steps of the $F_s(q_z, t)$ of the first layer do not show signs of time-scale separation with reducing temperature. On the contrary, τ_{c_3}/τ_{c_2} generally decreases with reducing temperature. The temperature dependence of the relaxation times is in favor of the gradual merging of the second and third steps upon reducing temperature. To better see the trend, we also fitted VFT functions on the relaxation times of the second and third steps. The fitted curves are shown as thin dashed curves in [Figure S11a](#). The parameters of the fitted VFT curves are: $T_0 = 130.0$ K, $B = 620$ K, and $\tau_\infty = 0.000165$ ns for the second step and $T_0 = 130.0$ K, $B = 555$ K, and $\tau_\infty = 0.1$ ns for the third one. It should be noted that the accuracies of the fitted VFT functions on the relaxation times of the first layer are lower than the VFT function fitted on the bulk relaxation times. Unlike the bulk liquid, at 170 K and 160 K, the relaxation times of the first layer are outside of the simulation window; even at 180 K full decay of the relaxation function can not be seen, despite more than 4 μ s run (see [Figure S8c](#)).

[Figure S11b](#) shows the values of A_2 and A_3 at different temperatures. The contributions of the second and third steps in the decay of the $F_s(q_z, t)$ of the first layer can be estimated from A_2 and A_3 . It seems that upon reducing temperature, A_3 increases and A_2 decreases; although on the low-temperature side of the graph, this trend can not be seen. It should be noted that at the lowest studied temperatures, the full decay of $F_s(q_z, t)$ of the first layer is not observed in the simulation window (see [Figure S8c](#)), and hence the fitting parameters have a rather high degree of uncertainty.

In the main text, we provide a short explanation for the merging of the second and third relaxation steps with reducing temperature. Here we continue the discussion. In bulk glass-forming liquids, with decreasing temperature, the process of small-scale movements in the cages becomes separated from the α -relaxation process. In this case, at low temperatures, the cages become rigid, and most (or all) particles perform rattling movements in the cages before α -relaxation happens. Close to an attractive solid surface, with *increasing* temperature, the second and third relaxation steps become more separated. At high temperatures, intermolecular packing (caging) barriers are lower than the energetic barrier for escaping from the surface, and hence most particles perform small-scale back-and-forth movements close to the surface before the process of escaping from the surface. At low temperatures, intermolecular packing barriers become very large, and few particles that can overcome these barriers can also overcome the energetic barrier for escaping from the

surface. This leads to the merging of the second and third relaxation steps close to the surface.

- [1] S. Pronk, S. Páll, R. Schulz, P. Larsson, P. Bjelkmar, R. Apostolov, M. R. Shirts, J. C. Smith, v. d. S. D. Kasson, Peter M, B. Hess, and E. Lindahl, Gromacs 4.5: a high-throughput and highly parallel open source molecular simulation toolkit, *Bioinformatics* **29**, 845 (2013).
- [2] A. Foroozani Behbahani and V. Harmandaris, Gradient of segmental dynamics in stereoregular poly (methyl methacrylate) melts confined between pristine or oxidized graphene sheets, *Polymers* **13**, 830 (2021).
- [3] S. Kim, J. Chen, T. Cheng, A. Gindulyte, J. He, S. He, Q. Li, B. A. Shoemaker, P. A. Thiessen, B. Yu, *et al.*, Pubchem in 2021: new data content and improved web interfaces, *Nucleic Acids Res.* **49**, D1388 (2021).
- [4] P. Scheidler, W. Kob, and K. Binder, The relaxation dynamics of a supercooled liquid confined by rough walls, *J. Phys. Chem. B* **108**, 6673 (2004).